Appl Phys B (2012) 107:539–549
DOI 10.1007/s00340-012-5001-1

Applied Physics B
Lasers and Optics

Measurement and simulation of rotationally-resolved chemiluminescence spectra in flames

A. Brockhinke · J. Krüger · M. Heusing · M. Letzgus

Received: 10 October 2011 / Revised version: 1 March 2012 / Published online: 21 April 2012

Abstract In recent years, there has been renewed interest in chemiluminescence, since it has been shown that these emissions can be used to determine flame parameters such as stoichiometry and heat release under some conditions. Even though the origin of these emissions has been known for a long time, little attention has been paid to the detailed analysis of the spectral structure.

In this contribution, we present rotationally-resolved spectra of all important chemiluminescent emissions OH A-X, CH B-X, CH A-X, and C_2 d-a in CH_4/air flames. A numerical model based on the LASKINν^2 code has been developed that allows, for the first time, to accurately predict the shape of the measured spectra for all of these transitions. Reabsorption of chemiluminescence within the emitting flame is shown to be a major factor, affecting both intensity and structure of OH^* spectra. Even in lab-scale flames, it might change the intensity of individual lines by a factor of 5. The shape of chemiluminescence spectra depends on several processes including initial state distribution and rotational and vibrational energy transfer (which, in turn, depend on the collisional environment and the temperature). It is shown that chemical reactions form OH^* in highly excited states and that the number of collisions is not sufficient to equilibrate the initial distribution. Therefore, high apparent temperatures are necessary to describe the shape of the measured spectra. In contrast, CH^* is formed with less excess energy and the spectral shape is very close to thermal. The rotational structure of C_2^* is close to thermal equilibrium as well. Vibrational temperatures are, however, significantly higher than the flame temperature. Implications and perspectives for flame measurements are discussed.

A. Brockhinke (✉) · J. Krüger · M. Heusing · M. Letzgus
Universität Bielefeld, Physikalische Chemie 1, Universitätsstraße 25, 33615 Bielefeld, Germany
e-mail: andreas.brockhinke@uni-bielefeld.de
Fax: +49-521-1062189

1 Introduction

Several molecular and radical species are formed in excited electronic states in flames. Their emissions, notably those of OH^* and CH^*, have been widely used for qualitative purposes, such as the visualization of flame structures. Much of the early work on these states has been summarized in the books of Gaydon and Wolfhard [23, 24]. However, once it has been established that chemiluminescent species are formed in side reactions constituting only a minor part of the overall combustion process and are usually only indirectly linked to the major reaction branches, there has been little interest to use them for quantitative measurements.

Recently, there has been renewed interest in using chemiluminescence for flame diagnostics—mainly driven by the demand for the online control of status and temporal development of instationary or oscillating combustion processes. These applications need fast, robust, and nonintrusive sensors [15]. Chemiluminescence of flames may provide a well-suited, low-cost inherent monitor of the combustion process [1, 8, 26, 28, 30, 39], since the emission of excited species from flames is intricately coupled to the flame chemistry. Chemiluminescence intensities and intensity ratios involving mostly OH^*, CH^* and C_2^* emissions have been analyzed and correlated to combustion properties such as stoichiometry and heat release, and this potential suggests their application in control.

The radiation emitted from chemiluminescent species is, however, the result of a complex interaction of reactive and non-reactive dynamic processes. Chemiluminescent species

are formed in chemical reactions which remain under investigation [3, 19, 44, 50]. The nascent energy distribution in the excited state is not known, and it is not directly reflected in the emitted chemiluminescence spectra under typical flame conditions, where collisional energy transfer plays an important role. Thus, the detected emission will be the result of the interplay of the *kinetic formation* and decay reactions with the *spectroscopic* effects of collisional quenching, electronic, vibrational, and rotational energy transfer (VET, RET). Investigation of these phenomena can profit from earlier studies of collisional effects in laser-induced fluorescence experiments [36, 37], with the difference, however, that instead of a single energy level in the excited state pumped by laser radiation, a distribution of states is populated as a consequence of chemical reactions.

In recent years, only few authors published chemiluminescence measurements with spectral resolution sufficient to allow insight into these processes [20, 32, 38]. Even in these cases, the major focus was the investigation of the correlation between chemiluminescence signals and flame parameters, and there was little discussion of the spectral structure.

Therefore, one goal of our study is to measure chemiluminescence of OH^*, CH^* and C_2^* with a spectral resolution high enough to allow identification of individual rotational lines and develop a numerical model that can accurately predict these spectra. This is a prerequisite for absolute concentration measurements of these species [43, 48, 52]. Since it has been reported [10, 46] that reabsorption can have a profound impact both on intensity and shape of the OH^* chemiluminescence, absorption spectra are measured as well. Implications for chemiluminescence measurements are discussed.

2 Experimental

Chemiluminescence emissions are mainly studied in flames of an atmospheric-pressure Hencken burner which consists of an uncooled, square matrix with an edge width of 25 mm. The matrix is filled with an honeycomb mesh that separately feeds both fuel and oxidizer gases to the burner. The individual flames on this burner are non-premixed and have a height of roughly 1 mm. Measurements are therefore conducted in the exhaust of the flame, where the Hencken burner provides near adiabatic flames over a wide range of equivalence ratios. Additionally, low-pressure flames at $p = 50$ mbar are studied on a homemade sintered bronze matrix burner with 63 mm diameter which is kept at 40 °C by means of thermostated water circulation. One advantage of these flames is that the shape of flame front can be resolved (which usually is not possible with chemiluminescence measurements in atmospheric-pressure flames) [39]. The burner is moved vertically for height-resolved scans. Gas flows are regulated by mass flow controllers (Mykrolis Tylan FC/DFC 2900/2910), calibrated flows are in slm (standard liters per minute at 1.013 bar and 0 °C). Low-pressure flames are diluted with a 1.1 slm argon flow.

For the chemiluminescence measurements, flame emissions are collected with a 50 mm diameter lens with focal length of $f = 500$ mm. Signals are imaged on the entrance slit of a 750 mm focal length monochromator (Acton Research SpectraPro 750). Detection is performed with an unintensified camera (Roper Scientific Pixis 256). Three gratings (150, 1800, and 3600 grooves/mm) are used to measure overview, moderate- and high-resolution spectra. Slit width of the monochromator was 50 µm in all cases. The setup permits to record spectra in the entire range from 200–1100 nm, which is typically covered in four portions. Integration times up to 5 minutes have to be used, depending on the resolution and the species under investigation. The spectra of OH^* are measured with the 3600 grooves/mm and the spectra of CH^* and C_2^* with the 1800 grooves/mm. The spectral response of the complete detection system is calibrated using spectra of a D_2 lamp (in the UV) and a halogen bulb (in the visible) as reference.

For the absorption measurements, light from a D_2 lamp (L.O.T. Oriel) is collimated with a $f = 200$ mm lens to a beam with a diameter of $\varnothing = 12$ mm. After passing the homogeneous exhaust zone of the Hencken burner (absorption path length $d = 25$ mm), it is focused on the entrance slit of the monochromator with a 50 mm diameter lens with $f = 500$ mm.

The spectral resolution was $\Delta\tilde{\nu} = 1.18\ \mathrm{cm}^{-1}$ both for the chemiluminescence and the absorption measurements when the grating with the highest resolution was used.

3 Chemiluminescence in flames

A typical emission spectrum observed in hydrocarbon flames in the ultraviolet (UV), visible, and near infrared (IR) region with medium resolution ($\Delta\lambda = 4$ nm) is shown in Fig. 1. Most prominent are the emissions of OH^* with a maximum intensity at about 309 nm and a smaller peak around 285 nm. Both originate from the $OH(A^2\Sigma^+)$ state and are mainly due to the (0,0) and (1,0) transitions to the ground state. At larger wavelengths, two bands are emitted by the CH radical. The one seen at a wavelength of 431 nm (originating from $CH(A^2\Delta)$) is the strongest and accounts for about 80 % of the total CH^* emissions. This luminescence is responsible for the blue color of the reaction zone in hydrocarbon flames. Around 390 nm, the much weaker emissions originating from $CH(B^2\Sigma^-)$ can be seen. Chemiluminescence of the Swan bands C_2 d-a (hereafter referred as C_2^*) is observed in the visible region of flame spectra between 436 nm and 564 nm, mainly in fuel rich gas mixtures.

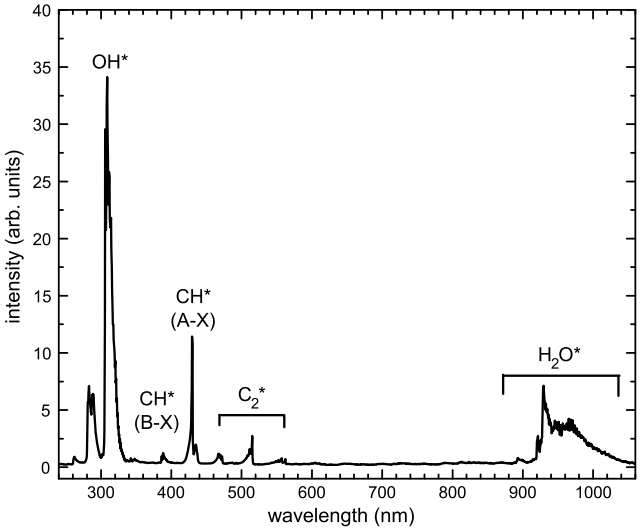

Fig. 1 Chemiluminescence of a CH_4/O_2 flame with 30 % H_2 addition

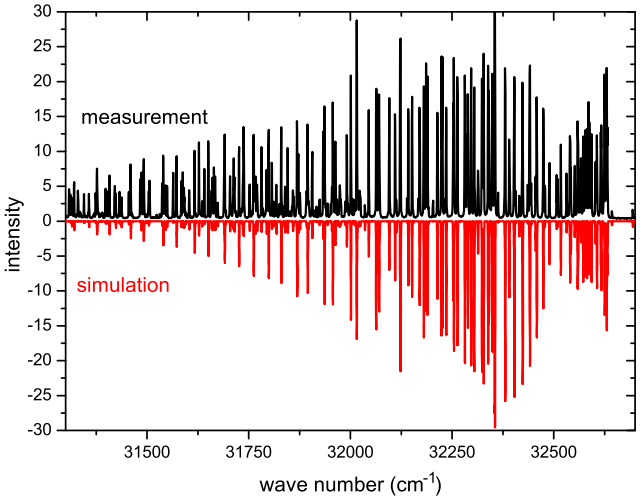

Fig. 2 *Top*: Highly-resolved OH emission spectrum in the flame front of an atmospheric CH_4/air flame. *Bottom*: OH emission spectrum at $T = 2000$ K calculated with LIFBASE [41]

The spectroscopic structure and the role of energy transfer in this band system has recently been analyzed in [7].

In the near IR, emissions from excited H_2O^* can be observed. They are strong in the IR and decrease in intensity in a stepwise fashion towards lower wavelengths. Although weak in the visible, they can be observed even at wavelengths around 750 nm and are responsible for the red color that can, e.g., be observed in H_2/O_2 flames. The states responsible for these emissions are, however, probably not populated by chemical reactions. In this energy region and at flame temperature, the Boltzmann fraction is 8×10^{-4}, so thermal excitation is the most likely origin.

It should be noted that other chemiluminescent emissions might be observed under different experimental conditions even though they did not play an important role here [23]. If higher excited states of the hydroxyl radical ($OH(B^2\Sigma^+)$ and $OH(C^2\Sigma^+)$) are populated, additional chemiluminescence signals will appear in the UV region below 280 nm. Emission originating from $CH(C^2\Delta)$ is even weaker than the CH B-X emission and is obscured by the strong OH* emissions in the region around 310 nm. In turbulent flames, especially at elevated pressure, CO_2^* chemiluminescence will play a role. CO_2^* is formed by a three-body reaction and its broad, featureless luminescence spans a wide spectral region from the UV to the IR with a maximum around 450 nm. In flames of nitrogen-containing fuels or with a high level of NO_x, NH* and CN* chemiluminescence can be observed at $\lambda = 337$ nm and 388 nm, respectively. Additionally, blackbody radiation will play a role for luminous, fuel rich flames.

4 OH* chemiluminescence

Figure 2 shows a highly-resolved OH emission spectrum obtained in the exhaust of an atmospheric-pressure CH_4/air ($\Phi = 0.8$) flame. The part of spectrum plotted comprises the $\Delta v = 0$ part of the OH A-X band, which contains more than 70 % of the OH emissions in the flames investigated here. The LIFBASE [41] simulation at the bottom of Fig. 2 shows the calculated emission spectrum at the flame temperature of $T = 2000$ K. Significant deviations can be seen: The simulation predicts well-defined bands with a maximum at rotational quantum numbers around $J = 7$ and a comparatively fast decrease toward higher quantum numbers. The spectral distribution observed experimentally is, however, completely different. Many more lines are visible in the measured spectrum and it is spread out significantly further; especially the lines with wave numbers below 31750 cm^{-1} which originate from states with high rotational quantum numbers are stronger than in the simulation (sometimes by more than a factor 4).

Therefore, it seems clear that modeling of OH* chemiluminescence is not possible by assuming a thermal distribution with the flame temperature. This has already been observed by numerous authors [9, 22, 33] who also discussed effects of pressure and fuel and oxidizer composition. Identifying the reason remained, however, under debate and comparisons between measured and modeled flame spectra are scarce.

The resolution of our measurements was sufficient to allow the determination of the strength of individual lines with different rotational quantum number. Figure 3 (solid black squares) shows a Boltzmann plot of rotational states in OH $A\,^2\Sigma(J)$. For a thermal distribution, a straight line would be expected with the slope being the product of the Boltzmann constant k and the flame temperature T. Figure 3 shows, that this is not the case for the observed OH* states. The curve roughly falls into two parts: One with a comparatively small slope at low rotational quantum numbers and a signif-

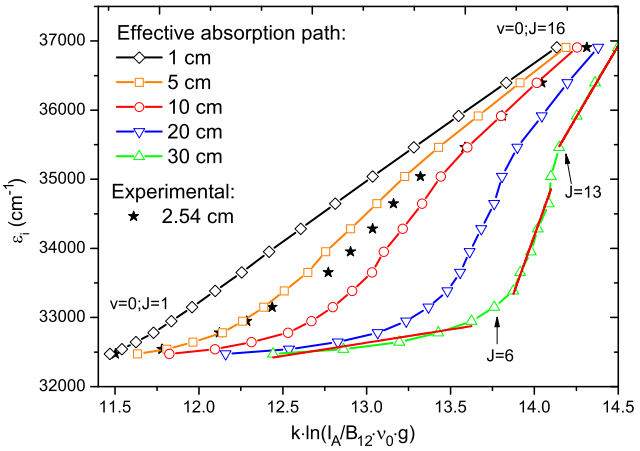

Fig. 3 Boltzmann plot of rotational states in OH A $^2\Sigma$(J). *Solid*: Measured in a Hencken flame. *Open symbols*: Simulated for several optical path lengths

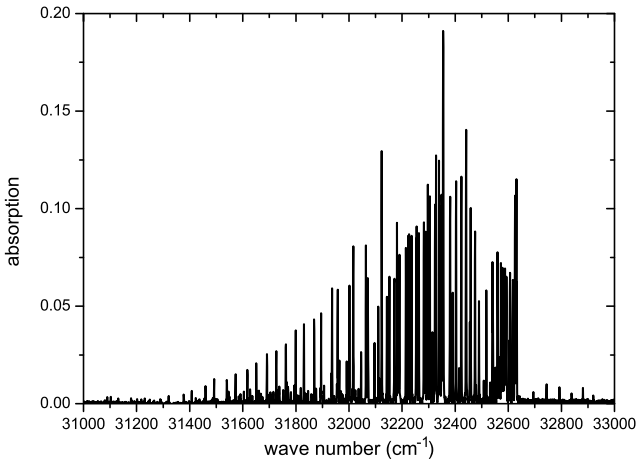

Fig. 4 Absorption spectrum obtained in a CH_4/air flame on a Hencken burner. All observed features are due to absorption in the OH A-X (0, 0) band

icantly steeper one for high quantum numbers. Therefore, the observed OH* spectrum cannot be described by a thermal distribution and it seems that the rotational states are not in equilibrium.

It is known, however, that absorption does not only affect the intensity of observed signals but can alter the shape of spectra as well. Since ground state mole fractions of OH frequently exceed 10^{-3}, the flame is not transparent. This has been observed numerous times [24] and is one of the reasons why quantitative laser diagnostic measurements are usually performed with excitation in the OH A-X (1, 0) band [17]. Therefore, a significant part of the emitted OH A-X (0, 0) chemiluminescence might be re-absorbed in the flame. Reabsorption will be strongest for the low to middle quantum numbers ($J = 2$–12), where the ground state population distribution of OH has its maximum.

In order to study this effect, we performed high-resolution absorption spectroscopy. Figure 4 shows an absorption spectrum obtained in a CH_4/air flame stabilized on a Hencken burner. All observed features are due to absorption in the OH A-X ($\Delta v = 0$) band. For the strongest transitions, absorptions up to 0.2 have been observed.

Due to the limited resolution of the measurement ($\Delta\tilde{\nu} = 1.18\ \mathrm{cm}^{-1}$), the real absorption of individual lines is, however, larger. Under our experimental conditions, the line width is dominated by Doppler-broadening and can be well described by a Gaussian function with a full width at half maximum of $\Delta\tilde{\nu} = 0.26\ \mathrm{cm}^{-1}$. The measured spectrum shown in Fig. 4 is in fact a convolution of the real spectrum and the experimental resolution. This convolution reduces the observed absorption.

Table 1 shows experimental values of the single-pass attenuation of several Q_1 lines of the OH A-X (0,0) branch in the methane flame where this effect has been taken into account. The absorption of the strongest line, $Q_1(7)$, is 0.686,

Table 1 Single-pass absorption and attenuation of several Q_1 lines of the OH A-X (0, 0) branch in the methane flame

J	Position (cm^{-1})	Absorption	Attenuation (%)
1	32474.56	0.228	40.8
2	32458.60	0.402	60.4
3	32441.82	0.532	70.6
7	32355.84	0.686	79.4
8	32327.98	0.642	77.2
11	32226.40	0.405	60.6
15	32045.32	0.129	25.7

which means that nearly 80 % of the light at this wavelength is absorbed by the flame. It can be seen that the signal attenuation exceeds 50 % at the positions of all strong lines. This, of course, decreases the total chemiluminescence intensity significantly, since these lines usually comprise the major contribution to the emission spectrum. In a recent publication, Sadanandan et al. report signal trapping on the order of 10 %–40 % for CH_4/air flames, which fits well with our measurements [46].

It should be noted that this significant absorption has been measured in the exhaust of a lab-scale flame (absorption path $d = 25$ mm). For larger flames, re-absorption will frequently become even more important, especially if the chemiluminescence emissions have to traverse a flame front or if combustion at elevated pressures is studied. OH* emissions observed from many large scale practical flames will therefore stem primarily from the edges of the flame as the light emitted in the interior does not escape the flame.

The absorption spectrum shown in Fig. 4 has also been used to experimentally determine the OH concentration and temperature of the flame under investigation. A temperature of $T = 2050 \pm 100$ K and OH mole fraction of 2.75×10^{-3}

has been obtained. Both values are not very accurate, especially since absorption is a line-of-sight technique and edge effects (e.g. cooling of the flame in the outer regions) have not been taken into account. They are, however, sufficient for the spectroscopic analysis presented in this paper, so no efforts have been undertaken to improve these estimates.

This strong reabsorption will affect the observed OH* chemiluminescence in several ways. Apart from the decrease in intensity mentioned above, the form of the spectra will change. Since "hot" lines originating from high-J states pass the flame nearly unaffected, these lines will become more pronounced. Additionally, a large part of the observed *total* chemiluminescence signal will originate from the outer layer of the flame, where re-absorption does not play a significant role.

To take this into account, the classical line-of-sight absorption described by the Beer–Lambert law $I = I_0 \times 10^{-A}$ is not adequate, since in our homogeneous flames, each part of the flame both absorbs and emits radiation. ELoSA (Emitting Line-of-Sight-Absorption) is a model which accounts for simultaneous emission and absorption on the path through the flame. Simple line-of-sight emission and absorption is assumed, so parameters specific to the detection geometry (F-numbers, etc.) are not taken into account. If the absorption $A(\lambda)$ of the whole path is $A(\lambda) = 0$ (transparent), the complete emitted intensity $I_0(\lambda)$ will reach the detector. In this case, an undisturbed emission spectrum will be measured. However, if the medium along the path with the length L has a specific wavelength-dependent opacity, the detector will see an undisturbed emission spectrum $I(\lambda)$ from $l = 0$ (outer flame layer) and a fully disturbed one from $l = L$ (flame position far away from detector). The detector then integrates all of the intermediate, position dependent disturbed emission spectra.

To take this ELoSA effect into account, the absorption spectrum of OH (X) convoluted with its molecular line width has to be calculated first. Afterward, the re-absorption effect can be quantified for each position in the flame and for every emission line (again convoluted with its line width) and the disturbed emission spectrum can be calculated.

Frequently, Boltzmann plots are used for the determination of the temperature. These Boltzmann plots require the knowledge of the population density of the desired system, for example some OH Q-lines. The measurement of the population density is affected by reabsorption as well, so we applied our ELoSA model to a simulated Boltzmann plot to investigate this effect. The reabsorption leads to virtually reduced population densities compared to the real undisturbed case. This virtual population densities are calculated applying ELoSA the line system under investigation. Results with different path length through the flame are shown in Fig. 3.

Using the ELoSA approach, a much better agreement between simulation and measured chemiluminescence spectra is obtained than by the simple approximation of a thermal distribution shown in Fig. 2. Additionally, the ELoSA model explains the characteristic non-linearity observed in the Boltzmann plot of the rotational states in OH A(J) (Fig. 3). Whereas a straight line is expected for a thermal distribution, the measurements show a bend at medium quantum numbers. This bend is well-reproduced by the ELoSA model (open symbols in Fig. 3) for an effective absorption path of about 2–5 cm, which fits well to the actual flame diameter of $d = 2.54$ mm. The effect becomes, of course, more pronounced when the absorption increases (shown in Fig. 3 for several path lengths).

However, there are still discrepancies between measurement and simulation both in the spectra and in the Boltzmann plots. At high rotational quantum numbers, absorption effects should become negligible and the observed distribution should converge against a straight line with the slope corresponding to the flame temperature. Figure 3 shows that this is not the case here, since the slope of the measured values is significantly steeper at high quantum numbers.

This deviation is also visible in the OH A-X (1,0) band around 35000 cm^{-1} (286 nm). Here, the absorption strength is a factor 3–4 weaker than for the 0,0 band due to different Franck–Condon factors. Therefore, re-absorption cannot be the reason for this behavior.

For an explanation, it has to be taken into account that OH* is produced by chemical reactions. Therefore, there is no reason that the initial state distribution should resemble a thermal Boltzmann distribution. In fact, it is much more likely that OH* is in a highly excited rotational and vibrational state after it is produced. Over time, however, collisions will equilibrate this initial distribution and the excess energy will dissipate. In most hydrocarbon flames, the dominant pathway for the formation of OH* is [11]:

$$CH + O_2 \rightleftharpoons CO + OH^* \quad (1)$$

The energy that is released in each collision complex can be calculated by adding the Gibbs enthalpy and the activation energy of the reaction [25]. For reaction (1), the activation energy is 0, and $\Delta_f H = 23490$ cm^{-1} ($\equiv$281 kJ/mol).

The consequence of this high excess energy is, that OH(A) may be formed in very high rotational and vibrational states. Energetically, even the formation of states with $v'' = 6$ is possible. However, vibrational levels with $v'' \geq 3$ (and higher rotational levels in $v'' = 2$) in the OH A-state are strongly influenced by pre-dissociation, which probably defines an upper limit of the states which are populated by the reactions. In rotational energy transfer, small steps are favored [6, 34]. In either case, it takes more than just a few collisions to equilibrate such a huge imbalance. Consequently, given the typical quenching-limited lifetime of OH in atmospheric-pressure flames of $\tau \approx 2$ ns [5] and typical collision times on the order of $\tau \approx 100$ ps, the state distribution in OH(A) will not equilibrate. This will affect the

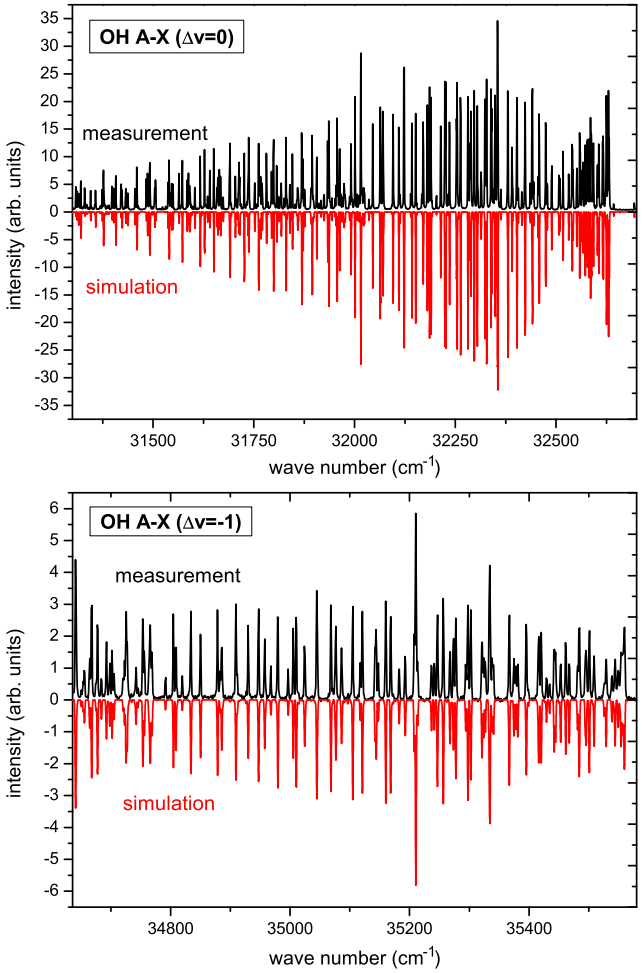

Fig. 5 Comparison between measurement (*black*) and simulation using the ELoSA program. *Top*: A-X($\Delta v = 0$), simulation with $T_{app} = 3000$ K. *Bottom*: A-X($\Delta v = -1$), simulation with $T_{app} = 4000$ K. A bath gas temperature of $T = 2000$ K has been used in both cases

rotational, and even more pronounced, the vibrational state distributions.

To take this nonequilibrium into account, we simulated OH* spectra with a high apparent temperature T_{app} in the excited state. Reabsorption was taken into account using the ELoSA model described above. For this, a ground state distribution with flame temperature ($T = 2000$ K) was assumed. Results are shown in Fig. 5. The upper panel shows the chemiluminescence spectrum in the region of A-X($\Delta v = 0$) compared with a simulation at $T_{app} = 3000$ K. The bottom shows the same comparison for the A-X($\Delta v = -1$) band, which is less affected by reabsorption. Here, an apparent temperature of $T_{app} = 4000$ K has been used.

It should be stressed, that the apparent temperatures are only fitting parameters and not real temperatures. Overall, Fig. 5 shows a very good agreement between measured and simulated spectra. The intensity of several small lines originating at higher vibrational levels is underestimated by the model, which indicates that an even higher temperature should be used to describe the vibrational state distribution. However, fitting with one or two apparent temperatures will always be an approximation, since the actual state dynamics is not adequately taken into account.

5 LASKINν^2 modeling

As described above, the spectral shape of chemiluminescence spectra can be modeled well by taking reabsorption into account and using an apparent temperature to account for the incomplete relaxation in the upper state. However, the model described in the previous section is partially empirical; especially, the apparent temperature which is necessary to fit the spectra will depend on the collisional environment.

A more complete model should take into account that chemical reactions typically create the excited state with a nonequilibrium state distribution. After that, relaxation processes including electronic quenching, vibrational, and rotational energy transfer (VET and RET, respectively) affect this initial distribution, and thus affect the measured spectra. This problem is similar to that encountered when performing quantitative laser-induced fluorescence (LIF) measurements. For LIF, a single rotational level in the excited electronic state of a molecule is usually populated with a laser pulse. Spectral shape and intensity of the measured fluorescence will depend on quenching, VET and RET.

The role of collisional energy transfer in LIF has been studied extensively for several molecules and radicals relevant for combustion, including OH [4, 6], CH [14], and C_2 [7]. We have developed a computer program, LASKINν^2 [40] that has proven to be capable of predicting the resulting fluorescence spectra with high reliability. It has recently been rewritten in C++ and a new differential equation solver (SUNDIALS) [31] has been added.

Chemiluminescence spectra are simulated using a modified version of LASKINν^2 [40]. Modifications have been introduced to describe the temporal and spectral development of an initial rotational distribution in the excited state of a chemiluminescent radical that encounters collisions with flame species under typical combustion conditions. The present version is capable of modeling the chemiluminescence of OH* A-X, CH* A-X and B-X and of C_2^* in the Swan bands. Also, CO_2^* emission as a broad spectral feature in the range of 280–600 nm has recently been analyzed and can be approximated by an empirical function. Population distributions in the excited state are modeled using from about 50 (OH*) to several hundred (C_2^*) quantum states, depending on the rotational constant. The rates for energy transfer between these states and quenching to the ground state depend on the flame composition and have been determined by laser-based experiments.

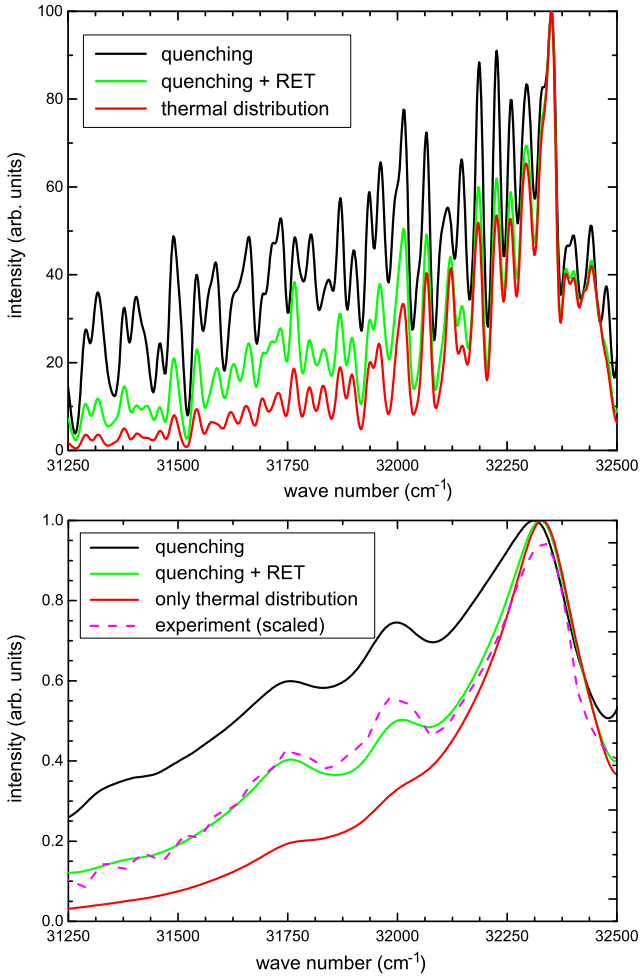

Fig. 6 Simulation of OH* chemiluminescence spectra assuming formation in the A state with $T_{\text{nascent}} = 5000$ K. *Black*: Only quenching is considered. *Green*: Quenching and rotational energy transfer is taken into account. *Red*: Emission spectrum of a thermal distribution with $T = 2200$ K. *Bottom*: Same spectra, convoluted with a Gaussian ($\Delta\tilde{\nu} = 100\ \text{cm}^{-1}$). This allows comparison with a measured spectrum (*magenta line*, *dashed*)

Figure 6 shows the simulation of an OH* chemiluminescence spectrum assuming formation in the A state with $T_{\text{nascent}} = 5000$ K. The collisional environment has been set to 80 % N_2 and 20 % H_2O with a bath gas temperature of $T = 2200$ K and a pressure of 1 bar. The spectra are convoluted with a Gaussian function with a width of $\Delta\tilde{\nu} = 20\ \text{cm}^{-1}$ and are normalized to their peak value (at $\tilde{\nu} = 32352\ \text{cm}^{-1}$).

Our model shows, that levels with low rotational quantum number are quenched first. Therefore, pure quenching (black curve in Fig. 6) leads to spectra with an even higher apparent temperature than the initial distribution at $T_{\text{nascent}} = 5000$ K. If, however, rotational energy transfer is taken into account as well, thermalization sets in, and the shape of the observed spectra (green curve in Fig. 6) becomes closer to the emission spectrum of a thermal distribution with $T = 2200$ K (red). Even though the relaxation processes are quite fast, complete thermalization is not reached. Especially the "hot" lines at low wave numbers in Fig. 6 are twice as intense as in the thermal spectrum.

LASKINν^2 captures important trends of the dependency of chemiluminescence spectra on environmental conditions such as bath gas composition, temperature, and pressure. It especially allows realistic predictions of the expected rotational structure and helps to explain the fact that high apparent temperatures are needed to fit chemiluminescence spectra (see Sect. 4 and Fig. 5). The bottom part of Fig. 6 shows a comparison of a measured with a modeled midresolution OH spectrum (resolution $\Delta\tilde{\nu} = 100\ \text{cm}^{-1}$). The agreement is quite satisfactory.

Simulations show that the form of the resultant spectra does not depend strongly on the initial state distribution (which, in the current model, is assumed to be thermal with a high T_{nascent}). To further improve the model, however, quantum chemical calculations or molecular beam experiments would be helpful. They could allow a detailed insight in which rotational and vibrational levels OH* is created preferentially. While RET is handled well by LASKINν^2, more information on collider-specific VET rates would be desirable. Also, intensities are not yet available on an absolute scale. Therefore, further experiments are needed to reliably describe chemiluminescence features from kinetic and spectroscopic principles rather than from empirical relations.

6 CH* and C_2^* chemiluminescence

Figure 7 shows chemiluminescence spectra of CH B-X, CH A-X and C_2. Experimental results are compared with simulations at the flame temperature $T = 2000$ K. The program for the spectral simulations bases on LASKINν^2 [40] for the calculation of energy levels. For these molecules, however, energy transfer is not taken into account and the plotted graphs are simple emission spectra assuming a thermal distribution of the states. We showed that for CH, simulations are identical with the output of LIFBASE [41]. Our model can, however, handle C_2^* spectroscopy as well. Matrix elements for C_2 are calculated using Brown's effective Hamiltonian [12] and the corresponding elements given in [13]. Molecular constants have been taken from [45, 51].

It can be seen that measurement and simulation agree quite well for all spectra shown in Fig. 7 and that non-equilibrium effects such as the high apparent temperature observed for OH*-spectra (see Sect. 4) are not observed.

For the CH(A) and CH(B) state, the vibrational constants ω_e are roughly 30 % less and the rotational constants B_e are 50 % less than for OH(A). Still, the energy differences between adjacent states are comparable to those of

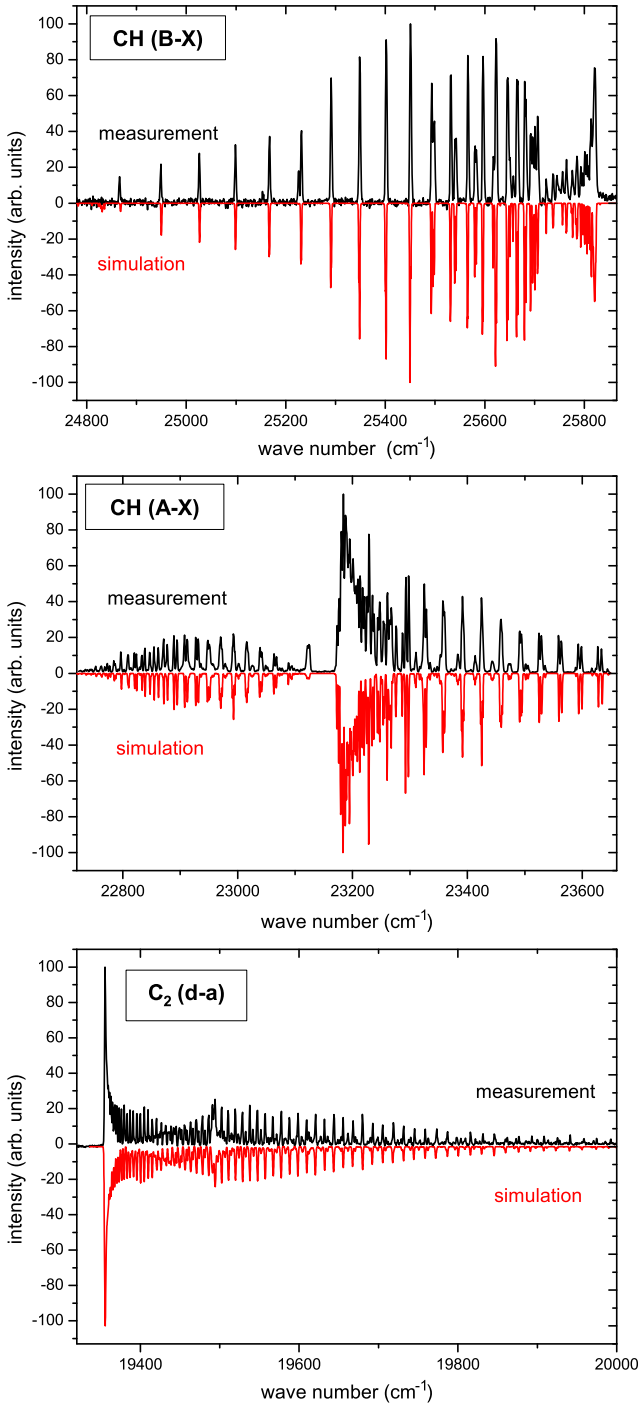

Fig. 7 Chemiluminescence spectra of CH B-X (*top*), CH A-X (*middle*) and C_2 (*bottom*). Experimental results are compared with simulations at $T = 2000$ K

OH, and VET and RET will of a similar order of magnitude. Therefore, faster energy transfer is not likely the reason for the finding that the population distribution in electronically excited states is in equilibrium with the surroundings.

It seems, that CH(A), CH(B), and C_2(a) are formed with less excess energy than OH(A) by their respective formation reactions. Therefore, fewer collisions suffice to create a rotational population that is nearly in perfect thermal equilibrium with the environment.

In literature, three different reactions are discussed for the formation of CH* [18, 23, 29]:

$$C_2 + OH \rightleftharpoons CO + CH^* \quad (2)$$

$\Delta_f H = 56508\ \mathrm{cm}^{-1}$ ($\equiv$676 kJ/mol),

$$C_2H + O_2 \rightleftharpoons CO_2 + CH^* \quad (3)$$

with $\Delta_f H = 7440\ \mathrm{cm}^{-1}$ ($\equiv$89 kJ/mol), and

$$C_2H + O \rightleftharpoons CO + CH^* \quad (4)$$

with $\Delta_f H = 5500\ \mathrm{cm}^{-1}$ ($\equiv$66 kJ/mol).

Hall et al. [29] stated that at atmospheric pressure and high temperatures (1200–2300 K) the most important formation reaction for CH* is reaction (4), followed by reaction (2). He concluded that reaction (2), which releases more than one order of magnitude more enthalpy than either of the other reactions, can be neglected if there is more C_2H than C_2 in the flame.

Our spectroscopic measurements support this finding. The excess energy of reaction (2) is equivalent to more than 56000 cm^{-1}. This is more than two times as much as that of reaction (1) which led to the considerable non-equilibrium effects and the high apparent temperatures observed in the OH* spectra. If reaction (2) would contribute significantly to the production of CH*, lines from very high rotational and vibrational states should show up. However, no such lines can be observed in Fig. 7.

Reactions (3) and (4) have, however, an excess energy of only 7440 cm^{-1} and 5500 cm^{-1}, respectively. This is much closer to the mean thermal energy of molecules in flames. Therefore, the energy which is available in the collisional complex, and thus the energy distribution of the produced CH* radicals will be close to thermal, which exactly fits to the observed spectra in Fig. 7.

The bottom panel in Fig. 7 shows that rotational fine structure of the observed part of the Swan bands C_2 d-a fits a thermal distribution as well. Reason for this is the fact that rotational energy transfer is much faster in C_2 than for CH and OH, since the vibrational constant B_e is only one-tenth of that for OH(A). Therefore, energy gaps between adjacent states are accordingly smaller, RET becomes more pronounced, and a faster thermalization occurs. This agrees well with our recent analysis of laser-excited C_2 in flames [7].

Analysis of the vibrational structure of the Swan bands gives, however, a different result. Significant deviations from a thermal distribution are observed, with a vibrational temperature T_{vib} between 4000 and 4500 K. This is not

as pronounced as in early investigations by Bleekrode [2] who observed vibrational temperatures between 9500 and 13000 K (more than a factor of three higher than adiabatic flame temperature and rotational temperature) in their low-pressure acetylene/oxygen flames.

The proposed formation reactions for C_2^* are [23, 27]:

$$CH_2 + C \rightleftharpoons H_2 + C_2^* \quad (5)$$

with $\Delta_f H = -303.6$ kJ/mol ($\equiv$25380 cm^{-1}), and

$$C_3 + O \rightleftharpoons CO + C_2^* \quad (6)$$

with $\Delta_f H = -345.5$ kJ/mol ($\equiv$28880 cm^{-1}).

These reactions form C_2 in the d-state with a high excess energy (very similar to that for the formation of OH*, reaction (1)). Therefore, the nonequilibrium effects discussed in detail for OH* (Sect. 4) can be observed in the vibrational structure of C_2^* spectra as well.

One aspect that facilitates the simulation of CH* and C_2^* emissions is, that reabsorption does not play a role here due to the low number density in their respective ground states. Typical peak concentrations of CH are about 3.5×10^{12} molecules/cm^3 in an stoichiometric atmospheric-pressure methane flame [21]. For rich low-pressure methane flames, the maximum concentration of C_2 is 1.5×10^{12} molecules/cm^3 [49]. OH concentrations are, in comparison, typically seven orders of magnitude larger (5×10^{19} molecules/cm^3 in atmospheric-pressure methane flames [35, 42, 47] and 6×10^{14} molecules/cm^3 in low-pressure methane flames [16]). Even though the concentration of both, CH and C_2, strongly depends on stoichiometry and the fuel type, they will remain significantly lower than that of OH in the Hencken flame studied here. Transitions strengths are of the same order of magnitude for all species discussed here. Therefore, it seems unlikely that reabsorption will play a role for CH* and C_2^* chemiluminescence even in the flame front of fuels known to produce comparatively large amounts of CH and C_2 and at elevated pressures.

7 Implications for flame measurements

Emissions originating from CH(A) and CH(B) are close to the thermal equilibrium. Measurement of these species is, therefore, straightforward and complicated only by optical factors (depth of focus, structure of the observed flame) which can, at least in principle, be corrected by methods such as tomography. Additionally, spatially-resolved measurements of the spectral shape of CH* and the rotational structure of C_2^* emissions and fitting to a Boltzmann distribution will provide a fair estimate of the local flame temperature.

This is, however, not an adequate treatment for OH*. The strong OH* ($\Delta v = 0$) emissions are not in thermal equilibrium and are severely affected by reabsorption. This leads to a complicated spectral structure characterized by a high apparent temperature. While we showed that the effect of reabsorption can be compensated in laminar flames of easy geometry, this will not be possible in turbulent flames.

Reabsorption might, however, prove to be beneficial for flame diagnostics under some circumstances. The ratio of OH* emissions in a spectral region which is strongly affected by reabsorption (such as the medium quantum numbers in the $\Delta v = 0$ band) and one that is less affected (e.g., the $\Delta v = -1$ band or lines with higher rotational quantum numbers) will be a function which allows to assess the relative importance of emissions from the center of the flame and its outer layers. Therefore, it might give an estimation of the flame surface, which is discussed as an important parameter for the characterization of turbulent flames.

For many practical chemiluminescence measurements, bandpass filters are used for the separation of the different chemiluminescence signals. Figure 1 shows that in clean methane flames, the contributions of the different species to the total spectrum show little overlap. Even the two CH* emissions from A- and B-state are separated by $\Delta\lambda \approx 40$ nm and can easily be measured independently. Therefore, it is possible to use bandpass filters that capture all emission of the desired chemiluminescent species while blocking all other light. In other flames, however, interfering emissions (e.g. CN*), broadband background (CO_2^*, black body radiation) or ambient light may prevent the use of such broadband filters.

Filters with a narrower bandpass add, however, a new complexity, as they will capture only part of the rotational spectrum of the species under investigation. Therefore, they will lead to an additional temperature dependency of the observed signal. Given the fact that temperature changes drastically between different flame conditions and, at least for OH*, the spectrum fits only to an apparent temperature which is difficult to obtain experimentally, it would be of considerable interest to find spectral regions where the measured intensity is directly proportional to the number density of the chemiluminescent species in question and does not depend on the temperature.

In order to find such detection intervals, we modeled OH* emission spectra with our software and plotted them versus the temperature in Fig. 8. All spectra have been normalized to the total intensity of the emitted spectrum, the line width of the simulation was matched to the experimental resolution (11.5 cm^{-1}). The blue curve shows the ratio between spectra obtained at $T = 1500$ K and $T = 2400$ K, respectively. If this ratio equals 1, the measured intensity at this spectral position is proportional to the total chemiluminescence emission and is independent of the temperature.

Figure 8 shows that such temperature invariant points do exist for OH at 307.3 nm and 312.4 nm. The second point is especially interesting since the slope of the intensity ratio

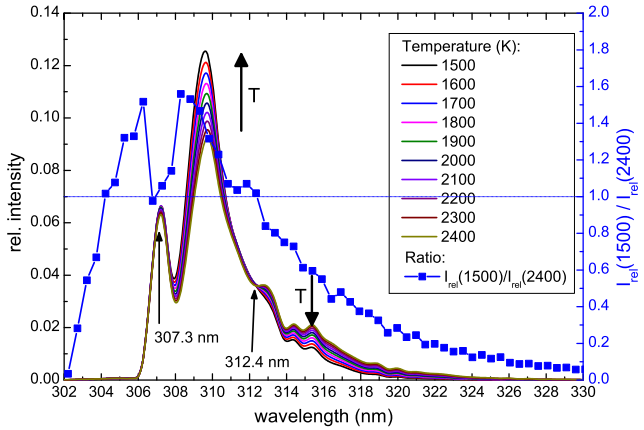

Fig. 8 Temperature dependency of the OH* emission spectrum as function of the temperature

is low at this spectral location. This means that the signal is temperature invariant even if a comparatively wide detection window is used. In this region, a mixture of lines with different quantum numbers contribute to the emission: P_1(7–9), P_2(8–10), Q_1(14–17), Q_2(13–16), and R_1(25–27). The net effect of this mixture of "cold" P and "hot" Q lines is the observed temperature invariance.

Similar temperature invariant points do exist for the other chemiluminescent species as well:

CH A-X: 436.7, 431, 429.5, 426.4 nm.

CH B-X: 440 nm

C_2: 513 and 559 nm.

Even though is seems intriguing to detect chemiluminescence in such spectral intervals where the measured intensity is directly proportional to the number density of the species in question, it remains to be shown if the temperature invariant points reported above can be useful for practical measurements. One problem is that very narrow-band, precise bandwidth filters are required, which are hard to obtain commercially. The technique can, however, easily be used for 1D chemiluminescence measurements with a spectrograph/CCD camera combination for detection.

8 Conclusions

Rotationally-resolved spectra of all important chemiluminescent transitions OH A-X, CH B-X, CH A-X and C_2 d-a have been measured in methane/air flames. In contrast to most previous investigations, our focus was to determine and interpret the shape of the observed spectra and discuss implications for flame measurements which are usually conducted with lower spectral resolution. The experiments are complemented with numerical modeling basing on the LASKINν^2 [40] code which, for the first time, can not only accurately predict the general shape but also the spectral fine structure of all chemiluminescent transitions.

The strongest chemiluminescence emissions are due to OH radicals in the $A^2\Sigma$ state with a maximum intensity around $\lambda = 305$ nm. Due to the high number density of OH in the ground state, significant reabsorption is observed. Even in the exhaust region of the small atmospheric-pressure flame investigated here, individual lines are attenuated by a factor of 5. Besides decreasing the signal strength, reabsorption also affects the spectral shape. Lines originating from rotational levels around $J = 7$ (which have the highest population at flame temperatures) suffer strongest. In consequence, emission of medium quantum numbers stems predominantly from the outer layer of the flame and lines originating from high rotational states become much more pronounced. This can be seen most clearly in Boltzmann plots of the observed line strengths, which deviate from the ideal straight line and exhibit a characteristic bend when re-absorption becomes significant.

We developed a computer program "ELoSA" which can take these effects into account for laminar flames. In contrast, measurements in turbulent flames will always be affected by reabsorption, especially at elevated pressures and for large burner dimensions. We suggested filter strategies where only the high rotational lines or OH* emissions around $\lambda = 286$ nm are detected, which are both affected less by reabsorption. However, both approaches will lead to a significant loss of signal. In an attempt to turn this problem into an advantage, we suggested a way to estimate the flame surface by relating the OH* emissions of spectral regions which are differently affected by reabsorption.

Even after taking reabsorption into account, the measurements could not be described by emission spectra at the actual flame temperature but required high apparent temperatures on the order of $T = 3500 - 4000$ K. This is due to the fact that OH* is formed in very high rotational and vibrational states by chemical reactions and the number of collisions is not sufficient to reach an equilibrium. First simulations with LASKINν^2 help to understand the effects of collisional processes on shape and intensity of chemiluminescence spectra. For a more detailed analysis, additional information on the initial state distribution is required, which is not available at present.

Chemiluminescence spectra of CH B-X, CH A-X and C_2 d-a are, on the other hand, much easier to interpret. Partially, this is due to the fact that ground state concentrations of CH and C_2 are so low that reabsorption does not play a role. On the other hand, we observed that these CH* chemiluminescence spectra are well described by simulations at the actual flame temperature. This implies that CH* is produced in states much closer to the thermal equilibrium than in the case of OH*. By using this information, we could argue that one of the reactions discussed for the formation of CH* does not play a significant role under our flame conditions. Due to fast RET, the rotational structure of C_2^* is close to thermal

equilibrium as well. Vibrational temperatures are, however, significantly higher than the flame temperature.

Acknowledgements The authors wish to acknowledge important contributions to the experiments described in this article by Dr. Regina Brockhinke and Angela Seipel. We thank Professor Dr. Katharina Kohse-Höinghaus for generous support and discussions. Elke Goos (DLR Stuttgart) contributed to the thermodynamic reaction analysis. Deutsche Forschungsgemeinschaft (DFG) has funded this work under contracts KO 1363/21-2, PAK 116/1 and 116/2 and SFB 686 TP C5.

References

1. F. Biagioli, F. Güthe, B. Schuermans, Exp. Therm. Fluid Sci. **32**, 1344 (2008)
2. R. Bleekrode, W.C. Nieuwpoort, J. Chem. Phys. **43**, 3680 (1965)
3. M. Bozkurt, M. Fikri, C. Schulz, Appl. Phys. B (2012, in press). doi:10.1007/s00340-012-5012-y
4. A. Brockhinke, K. Kohse-Höinghaus, Faraday Discuss. **119**, 275 (2001)
5. A. Brockhinke, M. Linne, in *Applied Combustion Diagnostics*. Taylor and Francis, New York (2002), pp. 128–154
6. A. Brockhinke, U. Lenhard, A. Bülter, K. Kohse-Höinghaus, Phys. Chem. Chem. Phys. **7**, 874 (2005)
7. A. Brockhinke, M. Letzgus, S. Rinne, K. Kohse-Höinghaus, J. Phys. Chem. A **110**, 3028 (2006)
8. K. Kohse-Höinghaus, A. Brockhinke, Combust. Expl. Shock Waves **45**, 349 (2009)
9. H.P. Broida, D.F. Heath, J. Chem. Phys. **26**, 223 (1957)
10. H.P. Broida, H.J. Kostowski, J. Chem. Phys. **25**, 676 (1956)
11. S.L.N.G. Krishnamachari, H.P. Broida, J. Chem. Phys. **34**, 1709 (1961)
12. J.M. Brown, E.A. Colbourn, J.K.G. Watson, F.D. Wayne, J. Mol. Spectrosc. **74**, 294 (1979)
13. J.M. Brown, A.J. Merer, J. Mol. Spectrosc. **74**, 488 (1979)
14. A. Bülter, U. Rahmann, K. Kohse-Höinghaus, A. Brockhinke, Appl. Phys. B **79**, 113 (2004)
15. S. Candel, Proc. Combust. Inst. **29**, 1 (2002)
16. S. Cheskis, Prog. Energy Combust. Sci. **25**, 233 (1999)
17. J.W. Daily, Prog. Energy Combust. Sci. **23**, 133 (1997)
18. K. Devriendt, H. Van Look, B. Ceursters, J. Peeters, Chem. Phys. Lett. **261**, 450 (1996)
19. J. de Vries, J.M. Hall, S.L. Simmons, M.J.A. Rickard, D.M. Kalitan, E.L. Petersen, Combust. Flame **150**, 137 (2007)
20. N. Docquier, S. Belhalfqoui, F. Lacas, N. Darabiha, Proc. Combust. Inst. **28**, 1765 (2000)
21. R. Evertsen, J.A. Van Oijen, R.T.E. Hermanns, L.P.H. De Goey, J.J. Ter Meulen, Combust. Flame **132**, 34 (2003)
22. A.G. Gaydon, H.G. Wolfhard, Proc. R. Soc. **199**, 89 (1949)
23. A.G. Gaydon, *The Spectroscopy of Flames* (Wiley, New York, 1974)
24. A.G. Gaydon, H.G. Wolfhard, *Flames, Their Structure, Radiation and Temperature* (Wiley, New York, 1970)
25. E. Goos, A. Burcat, B. Ruscic, New NASA Thermodynamic Polynomials Database With Active Thermochemical Tables updates, Report ANL 05/20 TAE 960, 2011
26. P. Gopalakrishnan, M.K. Bobba, J.M. Seitzman, Proc. Combust. Inst. **31**, 3401 (2007)
27. J. Grebe, K.H. Homann, Ber. Bunsenges. Phys. Chem. **86**, 587 (1982)
28. F. Guethe, D. Guyot, G. Singla, N. Noiray, B. Schuermans, Appl. Phys. B (2012, in press)
29. J.M. Hall, J. Vries, A. Amadio, E.L. Petersen, in *Aerospace Sciences Meeting and Exhibit*, vol. 43 (2005)
30. Y. Hardalupas, M. Orain, C.S. Panoutsos, A.M.K.P. Taylor, J. Olofsson, H. Seyfried, M. Richter, J. Hult, M. Aldén, F. Hermann, J. Klingmann, Appl. Therm. Eng. **24**, 1619 (2004)
31. A.C. Hindmarsh, P.N. Brown, K.E. Grant, S.L. Lee, R. Serban, D.E. Shumaker, C.S. Woodward, ACM Trans. Math. Softw. **31**, 363 (2005)
32. Y. Ikeda, J. Kojima, H. Hahimoto, Proc. Combust. Inst. **29**, 1495 (2002)
33. W.R. Kane, H.P. Broida, J. Chem. Phys. **21**, 347 (1953)
34. R. Kienle, M.P. Lee, K. Kohse-Höinghaus, Appl. Phys. B **63**, 403 (1996)
35. M. Köhler, A. Brockhinke, M. Braun-Unkhoff, K. Kohse-Höinghaus, J. Phys. Chem. A **114**, 4719 (2010)
36. K. Kohse-Höinghaus, J.B. Jeffries (eds.), *Applied Combustion Diagnostics* (Taylor & Francis, New York, 2002)
37. K. Kohse-Höinghaus, R.S. Barlow, M. Aldén, J. Wolfrum, Proc. Combust. Inst. **30**, 89 (2005)
38. J. Kojima, Y. Ikeda, T. Nakajima, Proc. Combust. Inst. **28**, 1757 (2000)
39. J. Kojima, Y. Ikeda, T. Nakajima, Combust. Flame **140**, 34 (2005)
40. M. Letzgus, A. Brockhinke, K. Kohse-Höinghaus, LASKINν^2, Bielefeld University, Chemistry Department, Physical Chemistry 1, available at http://pc1.uni-bielefeld.de/~laskin, 2012
41. J. Luque, D.R. Crosley, LIFBASE (version 2.0.6), Report MP 99-009, SRI International, Menlo Park, CA, 1999
42. X. Mercier, E. Therssen, J.F. Pauwels, P. Desgroux, Chem. Phys. Lett. **229**, 75 (1999)
43. P. Nau, J. Krüger, A. Lackner, M. Letzgus, A. Brockhinke, Appl. Phys. B (2012, in press)
44. E. Petersen, M. Kopp, N. Donato, F. Güthe, in *Proceedings of ASME Turbo Expo 2011 GT2011*, June 6–10, 2011, Vancouver, British Columbia, Canada (2011)
45. C.V.V. Prasad, P.F. Bernath, Astrophys. J. **426**, 812 (1994)
46. R. Sadanandan, W. Meier, J. Heinze, Appl. Phys. B **106**, 717 (2012)
47. A. Schocker, K. Kohse-Höinghaus, A. Brockhinke, Appl. Opt. **44**, 6660 (2005)
48. G.P. Smith, J. Luque, C. Park, J.B. Jeffries, D.R. Crosley, Combust. Flame **131**, 59 (2002)
49. G.P. Smith, C. Park, J. Schneiderman, J. Luque, Combust. Flame **141**, 66 (2005)
50. G.P. Smith, C. Park, J. Luque, Combust. Flame **140**, 385 (2005)
51. A. Tanabashi, T. Amano, J. Mol. Spectrosc. **215**, 285 (2002)
52. K.T. Walsh, M.B. Long, M.A. Tanoff, M.D. Smooke, Proc. Combust. Inst. **27**, 615 (1998)